Dalton Transactions

RSC Publishing

PAPER

View Article Online
View Journal | View Issue

Cite this: *Dalton Trans.*, 2013, **42**, 8328

Formation and characterization of thioglycolic acid–silver cluster complexes

Bruno Bellina,[a] Rodolphe Antoine,[a] Michel Broyer,[a] Lars Gell,[b] Željka Sanader,[c] Roland Mitrić,[d] Vlasta Bonačić-Koutecký[b,c] and Philippe Dugourd*[a]

Received 22nd February 2013,
Accepted 3rd April 2013

DOI: 10.1039/c3dt50485a

www.rsc.org/dalton

Gas phase reactivity observed in an ion trap was used to produce silver clusters protected with thioglycolic acid. Fragmentation pathways as well as optical properties were explored experimentally and theoretically. Sequential losses of SCH_2 and CO_2 in the ion trap lead to redox reactions with charge transfers between the metal part and the carboxylate and thiolate groups. This allows us to control the number of electrons in the metallic subunit and thus optical properties of the complexes. The presented formation process can be used as a prototype for tuning optical and chemical properties of ligated metal clusters by varying the number of confined electrons within the metallic subunit.

Introduction

The optical and electronic properties of noble metal nanoparticles and clusters have drawn considerable research interest due to possible applications in the fields of biosensing, single molecule spectroscopy and optoelectronics.[1,2] In a metal, conduction electrons are highly delocalized over large space, but in small nanoparticles and clusters, the decrease in size confines the electronic motion until separation of conduction and valence bands occurs and eventually molecular-like discrete electronic states and a nonzero HOMO–LUMO gap appear.[3–5] Their optical spectra display discrete visible or near-infrared absorption and emission bands, in contrast to optical spectra of large nanoparticles that are characterized by a broad band given by the surface plasmon resonance.[6] The order and spacing of the discrete levels depend on the structure of confinement and the number of electrons. Ligand-protected noble metal clusters are particularly attractive for applications,[3,7–10] such as optical labeling. In addition to protecting and to stabilizing the metal core, the ligands modify the dielectric constant at the surface of the metal core as well as the space in which the electrons are confined.[11] There may also be one or several electrons localized in metal–thiolate or metal–carboxylate bonds reducing the number of electrons in the metal core.[12,13] An alternative to the formation of protected clusters by wet chemistry is the synthesis of small and well defined organo-metallic cluster hybrids in gas phase. This approach was pioneered by the group of O'Hair[14–16] using gas phase sequential reactions by excitation of various precursor ions.[17]

In this paper, we study silver cluster protected with thioglycolic acid ligands in order to create species with a tunable number of electrons which are delocalized within the metal cluster subunit and we examine experimentally and theoretically their optical properties. Due to the large s–d energy gap in silver, the absorption at low energy in hybrid systems is mainly due to s-electron excitations within the silver subunit, in contrast to gold clusters where the relativistic effects responsible for the small s–d gap permit excitations of d electrons. The latter leads to optical transitions of similar intensities spread over a large energy interval while for silver a strong absorption in a narrow wavelength regime is observed.[18] Thioglycolic acid was chosen as a prototype ligand allowing for the joint experimental and theoretical investigations. It contains a thiol functional group and is soluble in water. We focus on clusters containing 3 and 4 silver atoms and use gas phase reactivity to produce species with different numbers of electrons which can be confined within the cluster subunit.

Materials and methods

Experimental

Thioglycolic acid (L = $HSCH_2COOH$) and $AgNO_3$ were purchased from Sigma Aldrich. The complexes were prepared by mixing a solution of 50 μM of $AgNO_3$ with 50 μM of thioglycolic acid in distilled water plus 2% of NH_3. Mass spectrometry and photodissociation measurements were performed using a

[a]*Institut Lumière Matière, UMR5306 Université Lyon 1-CNRS, Université de Lyon, 69622 Villeurbanne cedex, France*
[b]*Humboldt-Universität zu Berlin, Brook-Taylor-Straße 2, 12489 Berlin, Germany. E-mail: vbk@chemie.hu-berlin.de*
[c]*Center for Advanced Sciences and Technology (ICAST), University of Split, Meštrovićevo Šetalište bb., 2100 Split, Croatia*
[d]*Department of Physics, Free University Berlin, Arnimallee 14, 14195 Berlin, Germany. E-mail: philippe.dugourd@univ-lyon1.fr; Tel: +33 4 72 43 11 32*

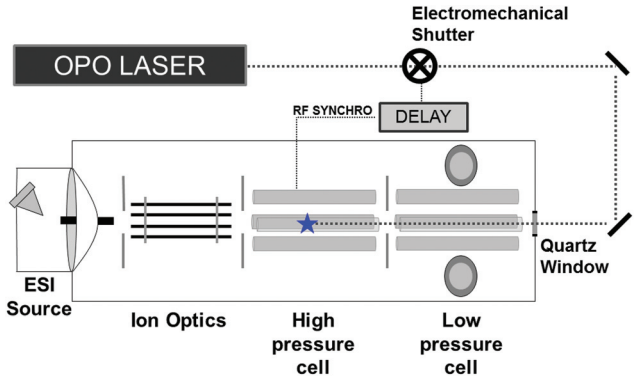

Fig. 1 Experimental set-up. Ions are irradiated in the high pressure cell.

modified LTQ Velos (Thermo electron) ion trap coupled to a tunable optical parametric oscillator (OPO) laser. Fig. 1 displays schematically the experimental set-up developed for this work. The laser is a nanosecond frequency-doubled tunable Panther™ EX OPO laser pumped by a Powerlite™ II Nd:YAG laser (both from Continuum, Santa Clara, CA, USA). The laser beam passes through two diaphragms (2 mm diameter) and lenses after which it is injected on the axis of the linear trap through a quartz window fitted on the rear of the LTQ Velos chamber. The collimation and focusing of the laser beam were optimized for maximal overlap between the laser beam and the ion cloud in the high pressure cell. It is then possible to select and excite the ions by laser and/or collision in this first linear ion trap (high pressure cell). An electromechanical shutter, electronically synchronized with the mass spectrometer, was placed along the laser beam and allowed to inject the laser light according to a given time sequence. To perform laser irradiation for a given period of time, we add in the ion trap RF sequence an MS^n step with an activation amplitude of 0%, during which the shutter located on the laser beam is opened.

The different species studied in this contribution were "synthesized" in the gas phase by successive sequences of collision induced dissociation (CID) of a silver–thioglycolic acid complex precursor (MS^n experiments). The different steps of ion selection and excitation are successively carried out in the high pressure cell. Final product ions are then transferred and mass analyzed in the low pressure cell. Photofragmentation yields at λ = 295, 355 and 440 nm were measured by irradiating ionic species for 500 ms (10 laser shots). The yield is defined as $\sigma = \ln(I0_{\text{precursor}}/(I_{\text{precursor}}))$ where $I0_{\text{precursor}}$ and $I_{\text{precursor}}$ are the intensities of the precursor ion signals recorded without and with laser irradiation.

Computational

Density functional theory (DFT) has been used to determine the structural properties of ligand-protected silver complexes employing the PBE0 functional[19] and the relativistic effective core potential (RECP) of the Stuttgart group for silver atoms.[20] The TZVP atomic orbital basis set was used for all atoms.[21] An extensive search for structures was performed using simulated annealing coupled to molecular dynamics (MD) simulations in the frame of the semiempirical AM1 method[22] with parameters for Ag atoms. The structures identified in this way were subsequently reoptimized at the DFT level using gradient minimization techniques, and stationary points were characterized by calculating the harmonic vibrational frequencies. Notice that low-energy structures obtained by DFT techniques differ substantially from those reached by the AM1 technique, in particular for larger complexes. Therefore, in spite of extensive search for the lowest energy structures, finding of the global DFT minimum is not fully guaranteed. The absorption spectra were computed employing the long-range corrected version of the hybrid B3LYP functional using the Coulomb-attenuated method (CAM-B3LYP),[23] which provides a reliable description of charge-transfer transitions. Molecular Dynamic simulations have been performed at the DFT level in order to understand the fragmentation processes and the electron transfers. Therefore MD simulation at constant energy with an initial kinetic energy of 5 eV was applied using the PBE functional and the SVP atomic orbital basis set for all atoms. The electron localization functions (ELF)[24] have been calculated in order to analyze the nature of bonding and the distribution of excess electrons within the cluster cores.

Results

The full mass spectrum (not shown) obtained after electrospraying the solution displays intense peaks corresponding to $[nL + (n + 1)Ag - (n + 2)H]^-$ anions, which may result from the formation of ···Ag–S–Ag–S–Ag··· chains. The peak corresponding to two thioglycolic acids and 3 silvers was selected and further fragmented by CID (Fig. 2). Successive losses of 44 and 46 uma are attributed to CO_2 and SCH_2 losses leading to a complex made of one thioglycolic acid and 3 silver atoms. Isolation and fragmentation of this latter complex lead also to the successive losses of 44 and 46 which corresponds to the formation of $[SCH_2 + 3Ag]^-$ and Ag_3^- ions (Fig. 2). To our knowledge, this is the first observation of the anionic Ag_3^- obtained

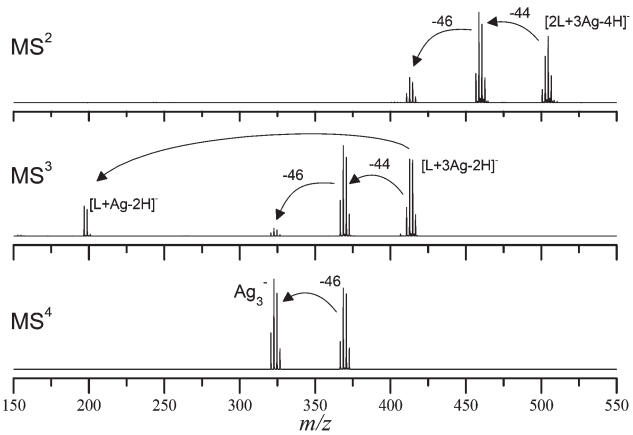

Fig. 2 MS^n spectra recorded after CID of $[2L + 3Ag - 4H]^-$.

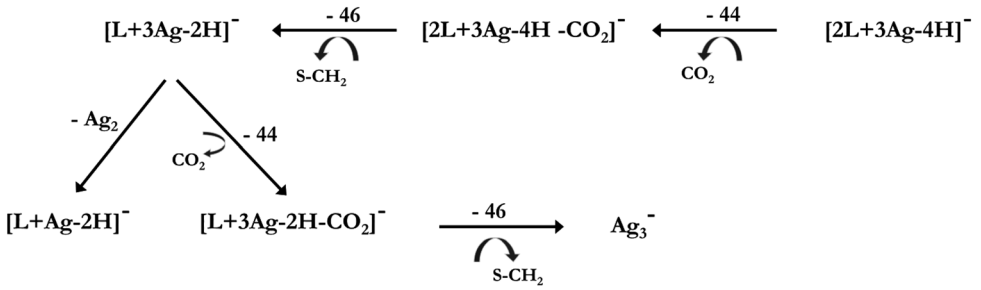

Scheme 1

through the fragmentation of small ligated metal clusters, while the formation of the cationic species *via* ESI/CID was reported in earlier work.[14,17] A loss of a silver dimer leading to the formation of an Ag–thioglycolic acid complex is also observed. Scheme 1 summarizes the fragmentation pathways obtained from MS^n experiments. Results of MD simulations starting from the $[2L + 3Ag - 4H]^-$ complex with a kinetic energy of 5 eV are shown in Fig. 3a. The initial structure is composed of a silver trimer with one ligand on each side. The structural properties are very similar to $[Ag_3 + 2GSH - 4H]^-$ (GSH glutathione peptide)[25] although the ligand is different. After 500 fs a loss of CO_2 is observed leading to the formation of a complex in which Ag_3 is bound to L – 2H on one face and SCH_2 on the other triangle face. At longer time the loss of SCH_2 is observed with the formation of the $[L + 3Ag - 2H]^-$ complex. The successive losses of CO_2 and SCH_2 observed along the MD trajectory are in full agreement with experimental findings and confirm Scheme 1. Fig. 3b shows structures and natural bond orbital (NBO) charges corresponding to the different equilibrium and transition state structures as well as their relative energies during the fragmentation process of $[2L + 3Ag - 4H]^-$. The decarboxylation obtained after excitation of the precursor ion ($[2L + 3Ag - 4H]^-$) results in the attachment of CH_2 to the silver trimer, which slightly reduces the net charge of the silver cluster from +1.69 to +1.39. Since this species is not the most stable isomer, it can undergo a reductive elimination reaction with a barrier of 1.48 eV forming an ester bond between the CH_2 and the COO groups. This leads to a silver cluster with a net charge of +0.3. Alternatively to this reductive elimination reaction, the loss of SCH_2 can occur forming $[1L + Ag_3 - 2H]^-$ over transition state (TS_3) that is significantly lower in energy than over the previous one (TS_2) as confirmed experimentally since the species with an ester bond has not been observed as pointed out later. Thus the energy profiles shown in Fig. 3b confirm the experimental finding that the loss of SCH_2 occurs preferably without formation of the ester bond leading directly to the formation of $[1L + Ag_3 - 2H]^-$ with two confined electrons.

For species containing 4 silver atoms, the complex made of 3 thioglycolic acids and 4 silver atoms was first selected in the full MS. After CID, successive neutral losses of CO_2 and SCH_2 were also observed. The spectra obtained after isolation and activation of the different intermediate species allow us to establish the fragmentation pathways described in Scheme 2.

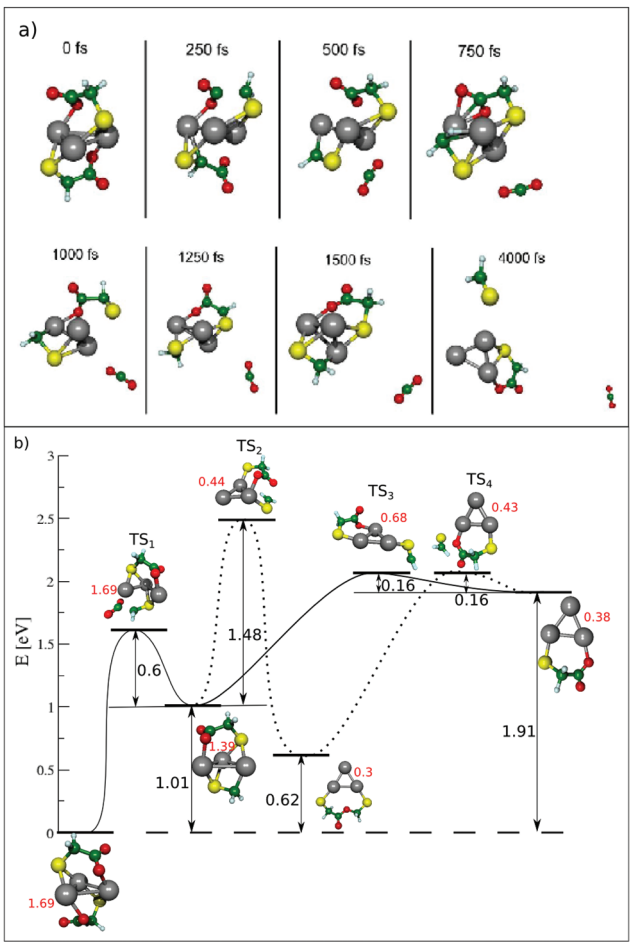

Fig. 3 (a) MD simulation starting from $[2L + 3Ag - 4H]^-$ at E = 5.0 eV. (b) Equilibrium and transition state structures, relative energies and NBO charges on a silver trimer starting from $[2L + 3Ag - 4H]^-$. The net charge of silver clusters is indicated in red.

The theoretical MD simulations confirm the first loss of CO_2 as shown in Fig. 4 while for the second loss of CO_2 and the subsequent loss of SCH_2 the simulations on a much longer time scale are needed. In the initial structure of $[3L + 4Ag - 5H]^-$ (*cf.* Fig. 4), two ligands are doubly deprotonated while the third one is singly deprotonated. The three thiolate groups and the two carboxylate groups are bound to silver. The first difference between Schemes 1 and 2 is that, in the case of 4 silver atoms, two CO_2 losses are observed before the loss of

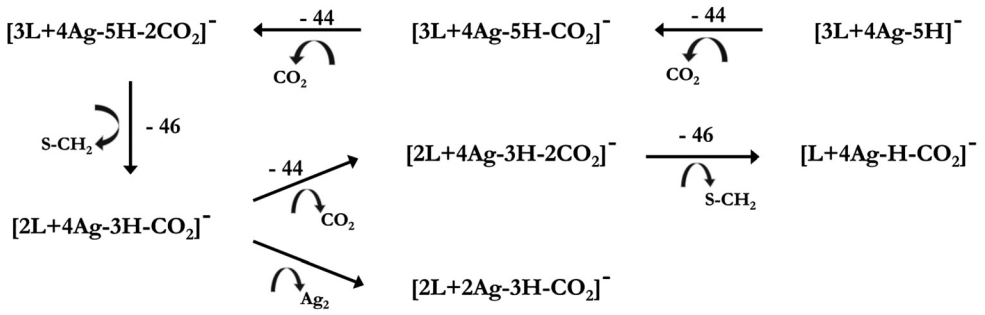

Scheme 2

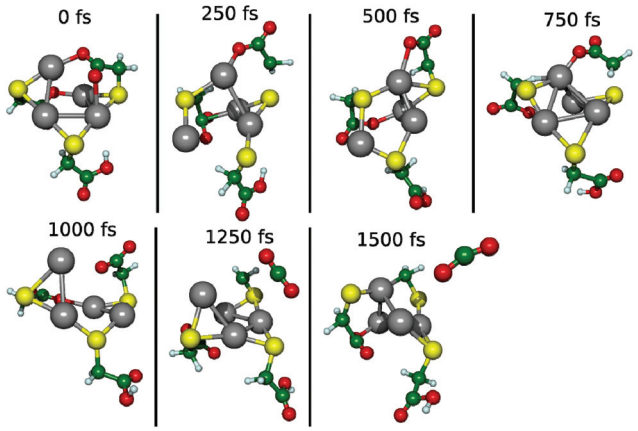

Fig. 4 MD simulation of the first decarboxylation of $[3L + 4Ag - 5H]^-$ at E = 5.0 eV.

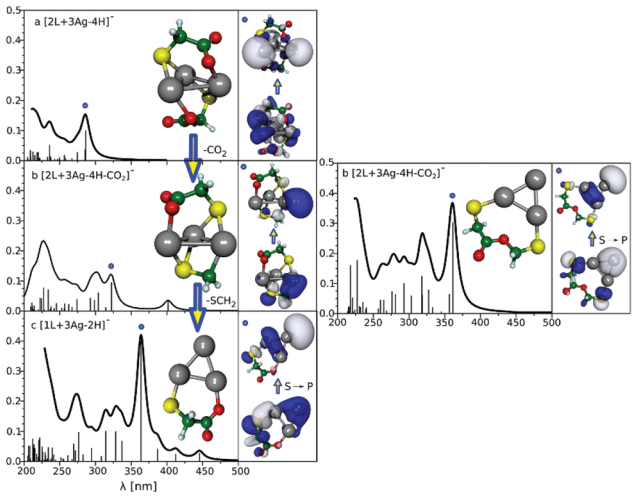

Fig. 5 Calculated spectra and transitions computed for a $[2L + 3Ag - 4H]^-$, b $[2L + 3Ag - 4H - CO_2]^-$ and c $[L + 3Ag - 2H]^-$. Orbitals for leading excitation corresponding to the marked transition are shown (cutoff for all orbitals is 0.025). Right panel corresponds to the structure of $[2L + 3Ag - 4H - CO_2]^-$ with an ester bond.

SCH_2. This reflects the higher strength of silver–sulphur bonds as compared to carboxylate–silver bonds. No ester bonds are formed after the first or second decarboxylation. Activation of the last complex is followed by the loss of Ag_2 or of the last CO_2 group followed by the loss of $S{=}CH_2$.

The optical spectrum calculated for the $[2L + 3Ag - 4H]^-$ complex displays a leading HOMO–LUMO excitation for transition at ~290 nm arising mainly from sulfur–silver binding orbitals to a linear combination of silver s-orbitals (*cf.* Fig. 5). After decarboxylation in principle two species can be formed. In the first species the ligands are bound above and below the Ag_3 plane, while in the second one an ester bond is formed between both ligands, bridging an Ag_3 subunit from the side. The absorption bands for the first species are red shifted. The first transition with low intensity appears at 400 nm and is due to excitation from the S–Ag and C–Ag bonds into the silver atom s orbital within the S–Ag–S bridge. The transition at 320 nm arises from the excitation from the S–Ag and C–Ag bonds into the silver atom s orbital bridging the sulphur and carbon atoms. The spectroscopic pattern of the second species in which an ester bond is formed is characterized by a strong transition at 360 nm (corresponding to S–P excitation within the cluster subunit). After loss of CO_2 and of the $S{=}CH_2$ part, the main feature in the optical spectrum is an intense S–P excitation at 360 nm accompanied by several weaker transitions at

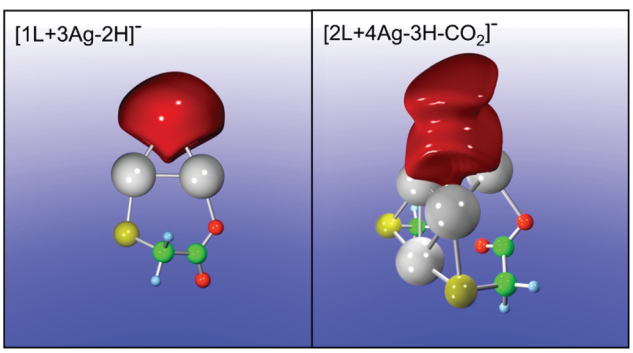

Fig. 6 Calculated electron localization functions for $[L + 3Ag - 2H]^-$ (left) and for $[2L + 4Ag - 3H - CO_2]^-$ illustrating confined electrons within the metallic subunit.

higher wavelengths. The position and oscillator strength of the S–P excitation are directly related to the confinement of two electrons in the silver subunit as illustrated in Fig. 6.

Experimental photofragmentation yields were measured for the three complexes ($[2L + 3Ag - 4H]^-$, $[2L + 3Ag - 4H - CO_2]^-$, $[L + 3Ag - 2H]^-$) at 3 wavelengths chosen to be

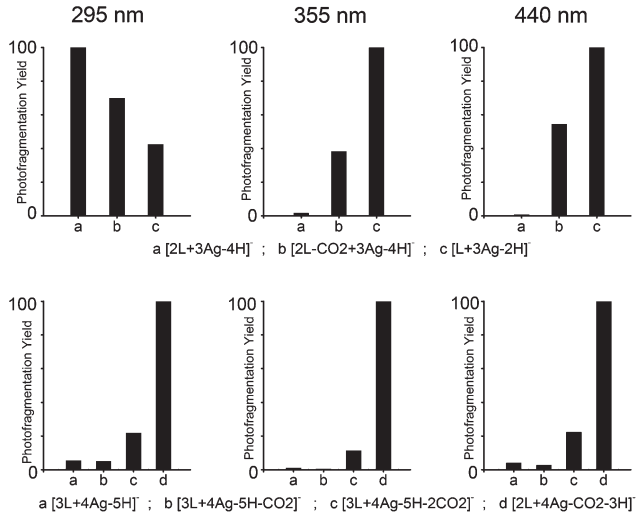

Fig. 7 Relative experimental photofragmentation yields recorded at 3 wavelengths. For each species the main relaxation channel is the loss of one electron leading to a neutral species. The photofragmentation yield is defined by $\ln(I0_{precursor}/(I_{precursor}))$ where $I0_{precursor}$ and $I_{precursor}$ are the intensities of the precursor ion signals recorded without and with laser irradiation.

discriminant for structural assignment. The main relaxation channel after photoexcitation is an electron loss resulting in a neutral species, which cannot be detected. In addition, ion products similar to those obtained after collisional excitation are observed, except for $[L + 3Ag - 2H]^-$) for which Ag_3^- is the only species obtained in the mass spectrum after photoexcitation (in addition to the electron loss). The total yield of fragmentation is obtained by comparing the intensity of the parent ion peak with and without laser irradiation. Results are shown in Fig. 7. According to calculations, at 295 nm, all complexes are expected to absorb. At 355 and at 440 nm, absorption is expected only for species with confined electrons. Experimental results confirmed that while the first species ($[2L + 3Ag - 4H]^-$) is not excited at 355 and 440 nm, the two others show electron loss (main relaxation channel) and fragmentation at these wavelengths. For $[2L + 3Ag - 4H - CO_2]^-$, the species with the ester bond does not show absorption at 440 nm which has been observed experimentally and corresponds to the transition calculated at 400 nm for the species without the ester bond (*cf.* Fig. 5b, left panel).

The theoretical absorption spectra of the initial species with 4 silver atoms and after the first decarboxylation are very similar as shown in Fig. 8 since the silver cluster subunit with confined electrons is not yet formed. No transitions above 260 nm are observed and the intense absorptions around 225 nm arise from binding Ag–S orbitals to mixed states composed of unoccupied cluster S, P and D orbitals. The most contributing excitations are shown on the right hand side of Fig. 8. The second decarboxylation gives rise to the transition which involves excitations from the bonds of SCH_2 to the silver cluster orbitals which is slightly red shifted to 280 nm. After the loss of SCH_2 three intense transitions arise at 456 nm, 388 nm and 321 nm corresponding to excitations from the

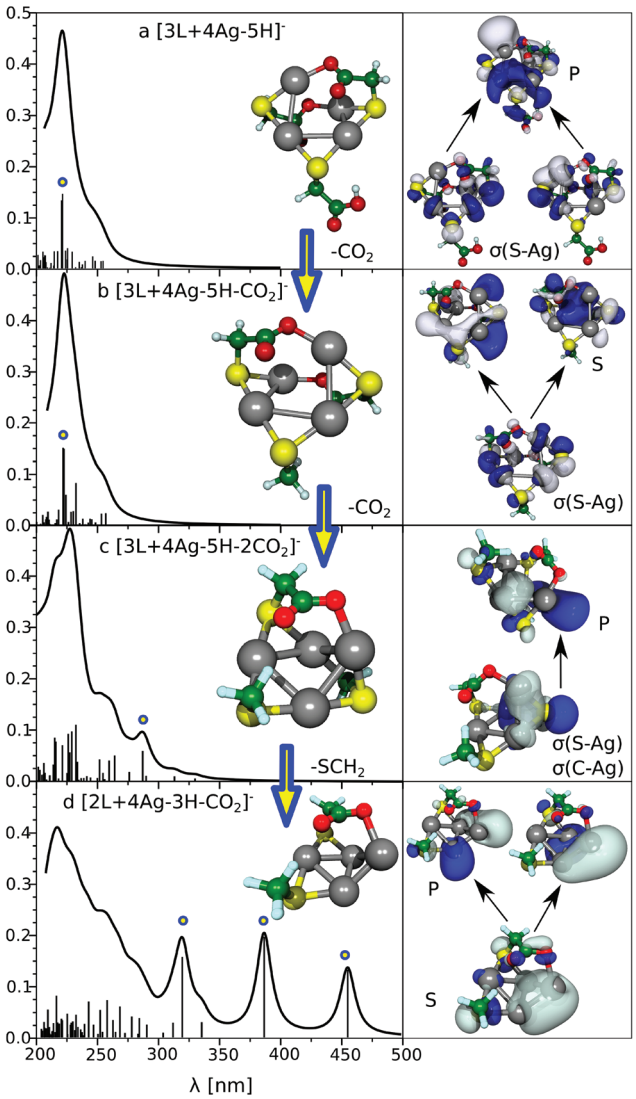

Fig. 8 Calculated spectra and transitions computed for (a) $[3L + 4Ag - 5H]^-$, (b) $[3L + 4Ag - 5H - CO_2]^-$, (c) $[3L + 4Ag - 5H - 2CO_2]^-$ and (d) $[2L + 4Ag - CO_2 - 3H]^-$. Orbitals for leading excitation corresponding to the marked transition are shown. For $[2L + 4Ag - CO_2 - 3H]^-$, two transitions for the 3 s–p type transitions are shown (the cut-off value for the orbitals was 0.025).

cluster S-orbital to the three cluster P-orbitals (only the first two are shown). Experimental results (Fig. 7) clearly show a strong increase in photofragmentation yield for the species $[2L + 4Ag - CO_2 - 3H]^-$ as compared to the yields recorded for the other species, which is in agreement with two confined electrons within the silver subunit as illustrated in Fig. 6.

Conclusion

Altogether, these results show that gas phase reactivity in an ion trap allows us to produce in a controlled way liganded metal clusters either without or with 2 electrons confined within the cluster subunit, exhibiting unique optical properties. Changes in the number of confined electrons occur

through a reductive elimination reaction with charge transfers between the metal part and the carboxylate and thiolate groups induced by losses of thiolate and carboxylic groups. The presented formation process can be used as a prototype for tuning optical and chemical properties of ligated metal clusters by varying the number of confined electrons.

Acknowledgements

The authors thank Franck Bertorelle for fruitful discussions during the course of this work. Financial support for the French-Croatian collaboration from CNRS (LIA NCBA) and French and Croatian Foreign Offices (Program Hubert Curien Cogito) is acknowledged. The Deutsche Forschungsgemeinschaft (DFG) in the frame of the "Emmy-Noether-Programme" (ENP-MI-1236) R.M. and Research Unit FOE1282 V.B.K. and R.M. is also acknowledged.

References

1 M. C. Daniel and D. Astruc, *Chem. Rev.*, 2004, **104**, 293–346.
2 P. K. Jain, X. Huang, I. H. El-Sayed and M. A. El-Sayed, *Acc. Chem. Res.*, 2008, **41**, 1578–1586.
3 S. W. Chen, R. S. Ingram, M. J. Hostetler, J. J. Pietron, R. W. Murray, T. G. Schaaff, J. T. Khoury, M. M. Alvarez and R. L. Whetten, *Science*, 1998, **280**, 2098–2101.
4 M. A. El-Sayed, *Acc. Chem. Res.*, 2001, **34**, 257–264.
5 W. A. de Heer, *Rev. Mod. Phys.*, 1993, **65**, 611–676.
6 T. G. Schaaff, M. N. Shafigullin, J. T. Khoury, I. Vezmar, R. L. Whetten, W. G. Cullen, P. N. First, C. Gutierrez-Wing, J. Ascensio and M. J. Jose-Yacaman, *J. Phys. Chem. B*, 1997, **101**, 7885–7891.
7 R. L. Whetten, M. N. Shafigullin, J. T. Khoury, T. G. Schaaff, I. Vezmar, M. M. Alvarez and A. Wilkinson, *Acc. Chem. Res.*, 1999, **32**, 397–406.
8 A. C. Templeton, W. P. Wuelfing and R. W. Murray, *Acc. Chem. Res.*, 2000, **33**, 27–36.
9 Y. Negishi, K. Nobusada and T. Tsukuda, *J. Am. Chem. Soc.*, 2005, **127**, 5261–5270.
10 R. Jin, *Nanoscale*, 2010, **2**, 343–362.
11 C. M. Aikens, *J. Phys. Chem. Lett.*, 2011, **2**, 99–104.
12 R. Hamouda, B. Bellina, F. Bertorelle, I. Compagnon, R. Antoine, M. Broyer, D. Rayane and P. Dugourd, *J. Phys. Chem. Lett.*, 2010, **1**, 3189–3194.
13 M. Walter, J. Akola, O. Lopez-Acevedo, P. D. Jadzinsky, G. Calero, C. J. Ackerson, R. L. Whetten, H. Groenbeck and H. Hakkinen, *Proc. Natl. Acad. Sci. U. S. A.*, 2008, **105**, 9157–9162.
14 G. N. Khairallah and R. A. J. O'Hair, *Angew. Chem., Int. Ed.*, 2005, **44**, 728–731.
15 C. Brunet, R. Antoine, M. Broyer, P. Dugourd, A. Kulesza, J. Petersen, M. I. S. Röhr, R. Mitric, V. Bonacic-Koutecky and R. A. J. O'Hair, *J. Phys. Chem. A*, 2011, **115**, 9120–9127.
16 G. N. Khairallah, T. Waters and R. A. J. O'Hair, *Dalton Trans.*, 2009, 2832–2836, DOI: 10.1039/b822371h.
17 T. Tabarin, A. Kulesza, R. Antoine, R. Mitric, M. Broyer, P. Dugourd and V. Bonacic-Koutecky, *Phys. Rev. Lett.*, 2008, **101**, 213001.
18 V. Bonacic-Koutecky, A. Kulesza, L. Gell, R. Mitric, R. Antoine, F. Bertorelle, R. Hamouda, D. Rayane, M. Broyer, T. Tabarin and P. Dugourd, *Phys. Chem. Chem. Phys.*, 2012, **14**, 9282–9290.
19 J. P. Perdew, K. Burke and M. Ernzerhof, *Phys. Rev. Lett.*, 1996, **77**, 3865–3868.
20 D. Andrae, U. Haussermann, M. Dolg, H. Stoll and H. Preuss, *Theor. Chim. Acta*, 1990, **77**, 123–141.
21 F. Weigend and R. Ahlrichs, *Phys. Chem. Chem. Phys.*, 2005, **7**, 3297–3305.
22 M. J. S. Dewar, E. G. Zoebisch, E. F. Healy and J. J. P. Stewart, *J. Am. Chem. Soc.*, 1985, **107**, 3902–3909.
23 T. Yanai, D. P. Tew and N. C. Handy, *Chem. Phys. Lett.*, 2004, **393**, 51–57.
24 A. D. Becke and K. E. Edgecombe, *J. Chem. Phys.*, 1990, **92**, 5397–5403.
25 B. Bellina, I. Compagnon, F. Bertorelle, M. Broyer, R. Antoine, P. Dugourd, L. Gell, A. Kulesza, R. Mitric and V. Bonacic-Koutecky, *J. Phys. Chem. C*, 2011, **115**, 24549–24554.